Scanning Electron Microscopy

Volume 1985
Number 1 *1985*

Article 41

11-23-1984

Progress in Element Analysis on a High-Voltage Electron Microscope

W. F. Tivol
New York State Department of Health

D. Barnard
New York State Department of Health

T. Guha
New York State Department of Health

SCANNING ELECTRON MICROSCOPY/1985/I (Pages 455-466)
SEM Inc., AMF O'Hare (Chicago), IL 60666 USA

0586-5581/85$1.00+.05

PROGRESS IN ELEMENT ANALYSIS ON A HIGH-VOLTAGE ELECTRON MICROSCOPE

W. F. Tivol*, D. Barnard, and T. Guha

Wadsworth Center for Laboratories and Research
New York State Department of Health
Albany, NY 12201

(Paper received March 26 1984, Completed manuscript received November 23 1984)

Abstract

X-Ray microprobe (XMA) and electron energy-loss (EELS) spectrometers have been installed on the high-voltage electron microscope (HVEM). The probe size has been measured and background reduction is in progress for XMA and EELS as are improvements in electron optics for EELS and sensitivity measurements.

XMA is currently useful for qualitative analysis and has been used by several investigators from our laboratory and outside laboratories. However, EELS background levels are still too high for meaningful results to be obtained. Standards suitable for biological specimens are being measured, and a library for quantitative analysis is being compiled.

KEY WORDS: microanalysis, high-voltage electron microscope, energy-dispersive x-ray spectrometer, biological analysis, thick specimens, background, brehmsstrahlung, shielding, probe size

*Address for correspondence:
William F. Tivol, Wadsworth Center for Laboratories and Research, New York State Department of Health, Albany, NY 12201
Phone No.: 518 474-6646

Introduction

Extension of XMA and EELS to HVEMs offers advantages of higher theoretical sensitivity and of greater allowed thickness for thin samples (as defined by Chandler, 1979). Although the cross-sections for the production of characteristic x-rays by electrons decrease as a function of electron energy in the 100 keV to 1200 keV range (Kobenstuedt, 1967; Bambynek et al., 1972), the cross-sections for brehmsstrahlung production decrease more rapidly and are more forward-peaked (Jackson, 1962) leading to a more favorable signal-to-noise ratio. Calculated signal-to-noise ratios at 200 keV and 1000 keV show an improvement by a factor of 3.4 which was confirmed experimentally by Cliff et al. (1978).

For 1000 keV electrons the practical limits on specimen thickness are set by absorption of characteristic x-rays or by the ability to obtain an electron image. Those limits are on the order of a few micrometers and vary somewhat depending upon the method of specimen preparation (which determines image properties) and the element(s) of interest (which determines absorption characteristics). The ability to examine thick and semi-thick sections greatly increases the accuracy and efficiency of determining ultrastructure in three dimensions (Rieder et al., 1984). The ability to perform chemical analysis and to correlate the chemical and ultrastructural information will further increase our understanding of many biological structures.

Other HVEMs have installed x-ray detectors (Doole, RC, Makin, J, Personal communication) or will soon do so (Pawley, J, Ackland, D, Personal communication); however, our detector geometry is unique. The detector is closer to the specimen than in other HVEMs giving both more signal and higher background. This geometry should be more useful for specimens where the element(s) of interest occur(s) in relatively small concentrations and where the characteristic peaks are in regions of low background.

We have analysed some standards at voltages ranging from 100 kV to 1200 kV in order to determine the limitations of our instrument, and we have examined a number of biological specimens which are representative of the kinds of specimen for which the element analysis capability of the HVEM is useful.

Materials and Methods

A Kevex energy-dispersive x-ray detector was specially designed for the AEI EM7 HVEM. The detector is mounted on a carriage which provides variable geometry; in the extended position, the detector is 16.8 mm from the sample, giving a solid angle of collection of 0.035 sr, and when fully retracted, the detector is clear of the specimen area so that it does not affect the normal operation of the microscope (see Fig. 1). The detector assembly is inserted through one of the eight ports giving access to the specimen area. A modified specimen translation ring was designed which incorporates a removable lead plug to shield the detector from stray radiation when it is not in use and a removable lead shroud to shield against multiply scattered radiation within the specimen chamber when it is in use. Figure 2 is a scale drawing of the translation ring showing bottom and side views and giving details of its construction. The ring is fabricated from phosphor bronze and rides on three teflon feet. The window labeled "x-ray detector" has a lead insert into which the shroud or the plug will fit. The plug is shown in the central area of the ring in position to be inserted and the shroud is shown at the bottom of the figure. Key-ways cut in the plug and shroud engage a bronze pin and a slight counter-clockwise turn locks either into the ring. After airing the column and removing the objective aperture and liner, the plug or shroud may be inserted or removed by means of a wand which will pass through the objective aperture port, located opposite the x-ray detector port. The objective aperture and liner are then reinstalled. The stage is inserted into the microscope so that the tip of the stage engages a cone (not shown) in the hole labeled "specimen support." The detector looks upward at a 15° angle and the specimen can be tilted at various angles to get the optimum signal-to-noise ratio. Figure 3 is a drawing of the microscope column showing the location of the x-ray detector and the electron energy-loss spectrometer. C1 and C2 apertures were designed which were made of aluminum and which were thick enough to absorb 1.2 MeV electrons. A series of lead disks was constructed which fit in the upper objective pole piece (see Fig. 1). Holes were drilled in the centers of the disks which were alternately the size of the hole in the upper objective pole piece, about 3 mm (1/8"), and about 1 mm (1/32") larger. When these were inserted in the pole piece, they provided about 22 mm (7/8") of lead with a crenellated central hole to minimize scattering from the sides of the hole. An aluminum disk about 3 mm (1/8") thick with a central hole about 3 mm (1/8") in diameter was inserted on top of the lead disks. A new C2 aperture holder was constructed of aluminum. Another aluminum disk about 3 mm (1/8") thick with a smaller central hole, 0.35 mm in diameter, was substituted for the first aluminum disk.

Probe size measurements were made by taking photographs of the focused beam. The photographs were taken at a series of exposures and magnifications which allow the determination of electron intensity over three or four orders of magnitude. For XMA and EELS measurements on our instrument, the second condenser aperture is 0.25 mm in diameter, the first condenser lens is maximally excited, and the gun bias voltage is minimal. These conditions give the least electron current and the smallest probe size. Spectra were obtained with these experimental conditions from aluminum vacuum-deposited to 100 nm thickness on a formvar-coated copper grid, from standards for the elements of biological interest in lithium borate glass obtained from C. E. Fiori (Fiori and Blackburn, 1982) and from several biological samples including thin (0.1 - 0.25 μm) and thick (1-10 μm) sections, both stained and unstained, and unsectioned material.

The electron energy-loss spectroscope has been installed (see Fig. 3) with a wire detector (Barnard et al., 1983). A major difficulty has been high background from electrons backscattered from the beam stop. Redesign of the beam stop incorporating a permanent magnet to reduce backscatter has lowered this background, and work is still in progress to reduce it further.

Results

It was hoped that the use of low-Z material would minimize brehmsstrahlung x-ray production, and that using apertures which could not be penetrated by the most energetic electrons would reduce stray radiation from electrons which are not focused into the beam. Neither of these hopes was fulfilled; the background with the new C1 or C2 apertures was worse than previously measured. A redesigned C1 aluminum aperture gave slight improvement as did an aluminum C2 aperture holder.

The stack of aluminum and lead disks gave excellent shielding at all voltages. Spectra were obtained from the 100 nm-thick aluminum specimen on a copper grid. The grid was secured by a Delrin circlip. This accounts for some of the minor peaks in Table 2, while others arise from parts surrounding the specimen area (e.g. pole pieces, specimen manipulators, etc.). The spectra are very clean (see Fig. 4 and Tables 1 and 2) even though the spectrum taken at 1.2 MeV had 85% dead time and shows evidence of pile-up. Even without special precautions, there is low background in our microscope arising from the specimen area in contrast to the situation at conventional voltages.

Table I gives the integrated net counts in the aluminum k-peak, the integrated background under the peak, the ratio of these two quantities and of the maximum peak height to the average background per channel. The first of these two ratios is a measure of the statistical error inherent in quantitation in the best possible case, and the second is a measure of qualitative detectibility. Table 2 gives ratios of net integrated counts in the $k_\alpha + k_\beta$-peaks for the elements Si, P, S, and Cl and of the net integrated counts in the k_α-peak for the elements K, Ca, Ti, Mn, Fe, Ni, and Cu to the net integrated counts in Al $k_\alpha + k_\beta$-peaks with Al normalized to 1000.

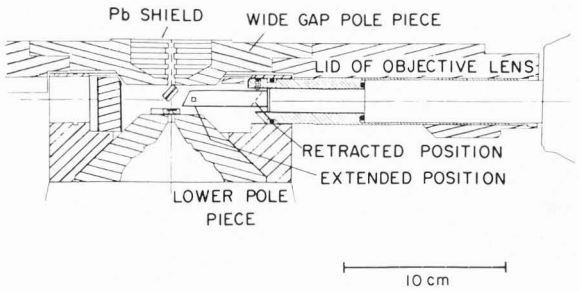

Figure 1. (Left) Specimen area of the high voltage electron microscope showing the location of the x-ray detector in the extended and retracted positions and the lead disks in the upper objective pole piece.

Figure 2. (Below) Specimen ring for use with the x-ray detector. Removable lead plug allows the detector to remain in the microscope column during normal operation. Dimensions in cm.

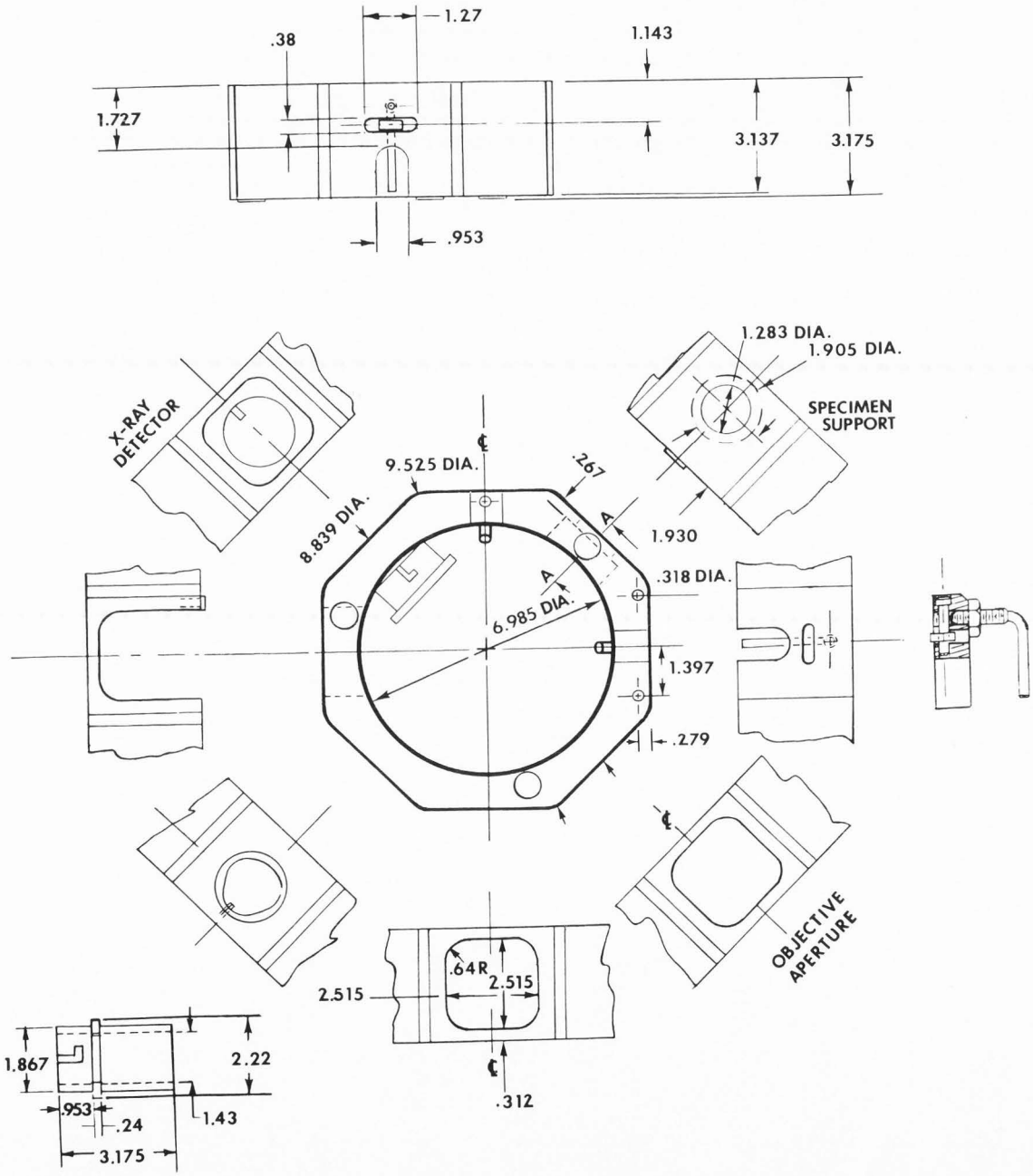

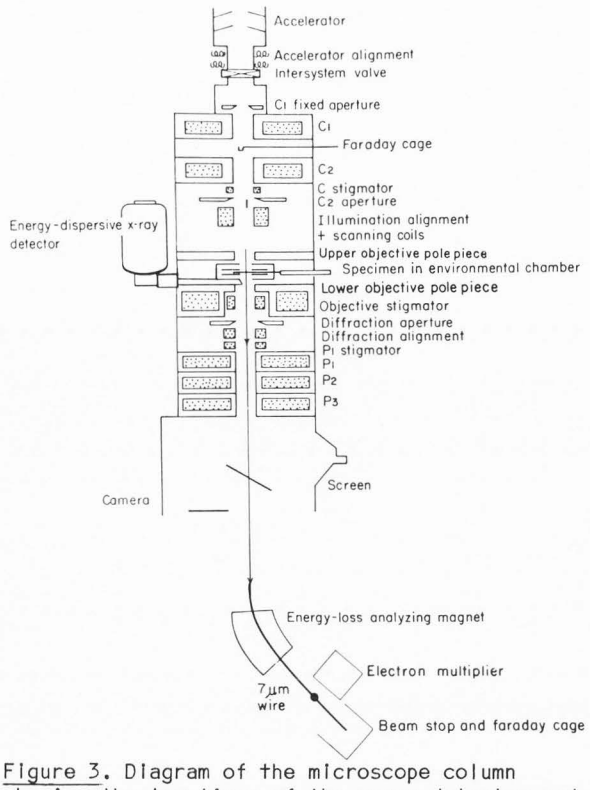

Figure 3. Diagram of the microscope column showing the locations of the x-ray detector and the electron energy-loss spectrometer.

Note that the ratio of the copper peaks to the aluminum peak generally decreases with increasing electron energy (except at 1200 kV where there are other problems with the spectrum). The very small signals produced by the Delrin clip also decrease generally with increasing energy.

Figure 5 shows the beam intensity profile for the conditions routinely used for XMA at 1000 kV on our instrument. Figures 6 and 7 show spectra and micrographs of several biological specimens, Figure 8 shows spectra from an air pollution particulate, background, the subtracted spectrum, the image and electron diffraction pattern of the particulate, and Figure 9 shows a spectrum of standard K1672 (Fiori and Blackburn, 1982), a lithium borate glass containing 2.38 weight percent P and 3.18 weight percent Ca. All the elements of interest from Na to U have been seen wherever they were expected. The probe is small enough to obtain significantly different spectra from areas separated by only a fraction of a micron (0.25 μm in 6b).

The aluminum disk with a smaller central hole lowered further the background arising from the upper part of the column (see Tables 3 and 4). Furthermore, none of the minor peaks found with the larger-bore aluminum disk (see Table 2) were found when the smaller-bore disk was used.

Discussion

Reduction of background levels is in progress for both XMA and EELS. We have been sufficiently successful in the case of XMA so that

Table 1. Peak-to-background ratio of Al k-peaks as a function of accelerating voltage

Accelerating voltage (kV)	400	500	600	700	800	900	1000	1100	1200
Integrated net counts	128959	354617	325039	230807	208590	224456	343460	387886	408860
Integrated background	10962	35728	27958	18414	19710	30653	43008	55890	82632
P/B ratio	11.76	9.93	11.63	12.53	10.58	7.32	7.99	6.94	4.95
Peak height to average background height ratio	60.23	49.49	60.06	63.55	51.55	38.90	48.62	45.24	23.73

Table 2. Ratios of counts in k-peaks as a function of accelerating voltage. Al = 1000

Accelerating voltage (kV)	400	500	600	700	800	900	1000	1100	1200
Element									
Si	4.79	3.33	2.26	3.73	2.43	1.14	ND*	ND	ND
P	2.88	1.17	1.33	1.55	1.54	ND	ND	ND	ND
S	6.58	6.90	4.27	4.22	4.26	4.43	4.44	3.08	ND
Cl	11.23	13.05	6.85	4.57	6.74	8.24	4.83	ND	ND
K	7.08	7.96	3.69	2.57	3.74	3.41	2.57	ND	ND
Ca	3.01	2.34	1.32	1.09	2.16	1.78	1.02	0.48	ND
Ti	2.19	2.62	0.61	ND	ND	ND	0.76	ND	ND
Mn	1.53	1.03	0.71	ND	ND	ND	ND	ND	ND
Fe	7.82	5.69	3.85	2.16	2.68	2.64	1.90	ND	ND
Ni	2.21	ND	ND	ND	ND	ND	ND	ND	ND
Cu	145.96	143.60	120.86	96.86	88.47	98.75	97.03	78.46	106.18

*ND = not detected.

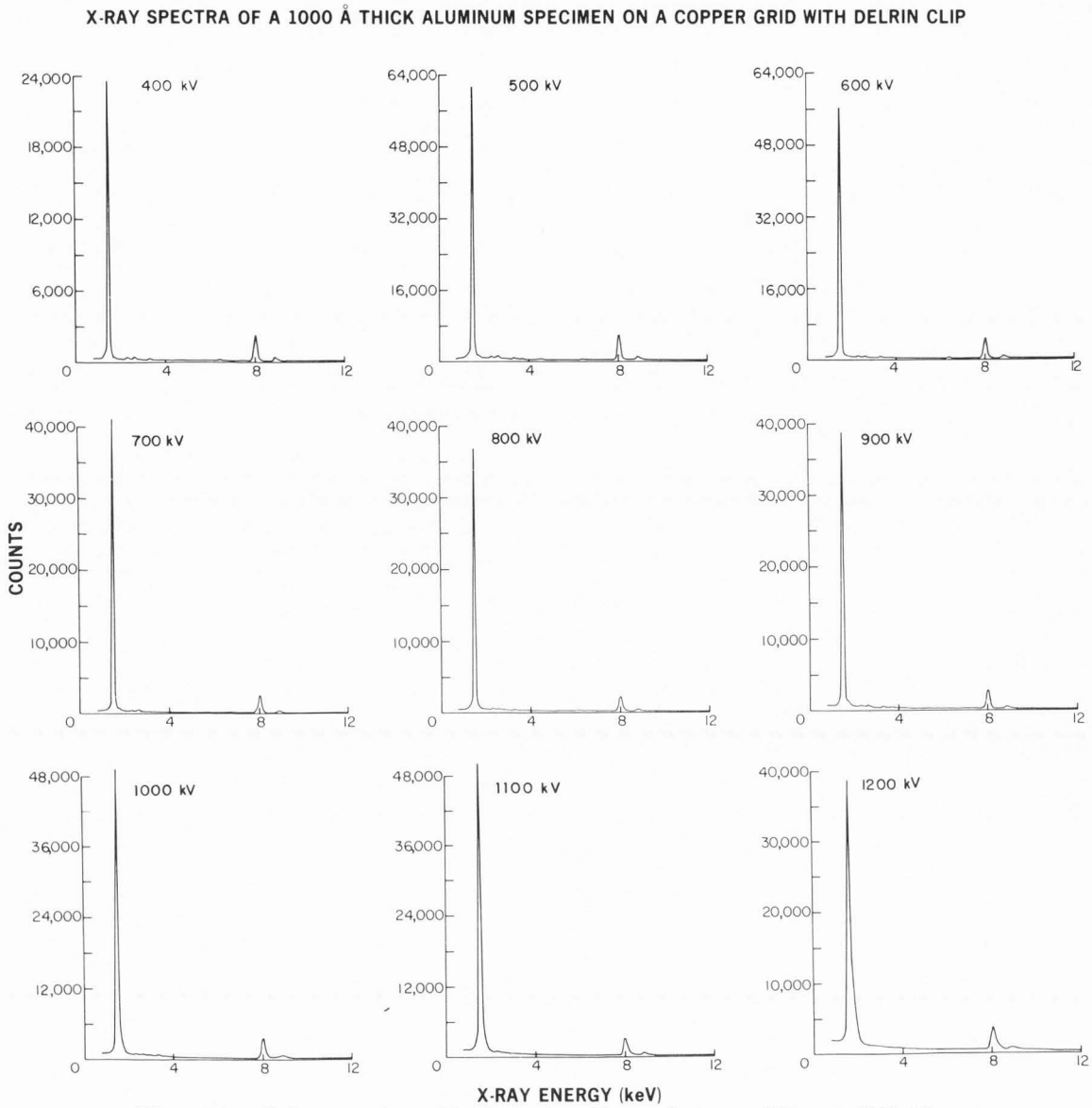

Figure 4. X-Ray spectra obtained at voltages between 400 and 1200 kV.

Table 3. Peak-to-background ratio of Al k-peaks as a function of accelerating voltage. Small bore aluminum shielding disk used.

Accelerating voltage (kV)	100	200	300	400	500	600	700	800	900	1000	1100	1200
Integrated net counts	500122	517694	508158	559676	493933	491269	490888	480569	658499	501708	535033	609871
Integrated background	45816	38952	35910	47385	31824	36456	33332	42100	62166	51459	68832	101061
P/B Ratio	10.92	13.29	14.15	11.81	15.52	13.49	14.73	11.41	10.59	9.75	7.77	6.03
Peak height to average background height ratio	47.95	60.19	55.64	55.38	76.39	62.41	73.90	56.81	47.84	47.11	37.32	26.38

Table 4. Copper k_α-peaks as a function of voltage. Al = 1000 Small bore aluminum shielding disk used.

Accelerating voltage (kV)	100	200	300	400	500	600	700	800	900	1000	1100	1200
Net Cu k_α-peak	82.05	71.21	55.97	58.05	40.67	44.32	37.48	65.63	49.23	37.99	36.92	43.20

the system is qualitatively useful. Shielding the x-ray detector against stray radiation has proved to be a formidable task (Doole, RC, Makin, J, Personal communication). The two sources of stray radiation are the upper part of the column and scattering within the specimen chamber. At conventional voltages (100 kV or less) contributions from these sources are roughly equal (Headley and Hren, 1978, Zaluzec, 1978, Bentley et al., 1979).

Since the replacement of high-Z material with aluminum gave no benefit if the aluminum was significantly thicker than the high-Z material, it was concluded that geometry is more important than material in the production of stray radiation by apertures.

The low observed value of background arising from scattering within the specimen area is probably due to the relativistic kinematics of higher energy electrons and the consequent forward peaking of scattering, but the geometry of the specimen area may also play a role, since distances are larger than in a conventional instrument and thus solid angles subtended by possible scattering and fluorescence sources are less. The decrease noted in the signals from minor components in the spectra of the aluminum standard as the energy of the incident electron beam is increased (See Fig. 4 and Table 2) supports the hypothesis that the forward peaking of the scattering is the reason for this low background component.

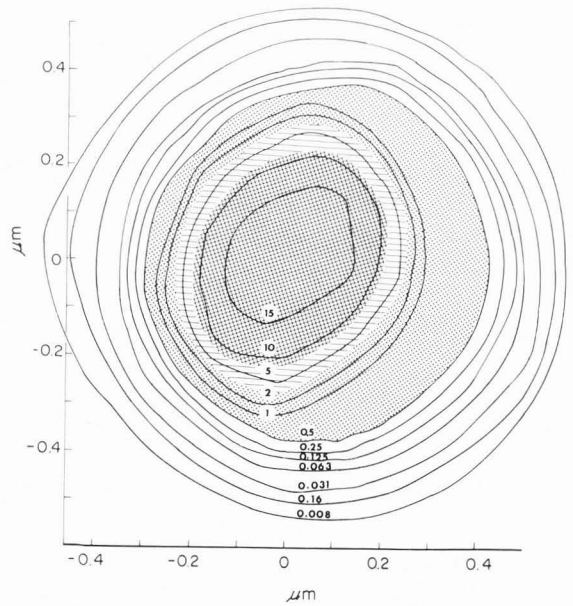

Figure 5. Intensity profile of electron beam: 0.25 mm C2 aperture, C1 = 24, bias = 1, voltage = 1 MV, arbitrary intensity units. The cross hatched area contains 75%, the lined area 90%, and the stippled area 99% of the electron intensity.

The changes in peak-to-background ratios and in ratios of minor components to aluminum in Tables 1 and 2 are consistent with a decreasing background component produced by multiple scattering within the specimen area combined with increasing production of peak and background counts generated by stray radiation as the accelerating voltage is increased.

Although the minor components seen when the larger-bore aluminum disk was used were produced by stray radiation, since they were not seen when the smaller-bore disk was used, there appears to be at least a significant fraction produced by multiple scattering, otherwise the ratios of these peaks to the aluminum peak would increase

Figure 6. (Top of next page) X-ray spectra of several biological specimens. a) Platinum deposit in feline sensorimotor cortex (Agnew WF, Personal communication), b) Inner and outer edges of the skin of an untreated Tradescantia paludosa pollen grain (Mascarenhas J, Personal communication), c) Aluminum inclusion and silver-stained area of rabbit brain stem (Moretz RC, Personal communication), d) Unstained, freeze-dried rat kidney proximal tubule (Wedeen R, Personal communication), e) Unstained rabbit brainstem (Moretz RC, Personal communication), f) $NaSb(OH)_6$ precipitate in rabbit cornea (Kaye et al., 1965).

Figure 7. (Bottom of next page) Micrographs of specimens corresponding to spectra in figure 6. a) Pt 30% Ir microelectrode implanted and pulsed with 3.2 mC/cm^2; tissue perfused with 3% glutaraldehyde plus 2% paraformaldehyde in phosphate buffer then stained with lead citrate and uranyl acetate; 1 μm section (unpublished work), b) T. paludosa pollen grain placed on grid, c) rabbit injected in cisterna magna with a slurry of aluminum in saline then perfused intracardiac with 3% glutaraldehyde in 0.1 M phosphate pH 7.4 saturated with H_2S; tissue chopped to 50 μm blocks and subjected to modified Timm's AgS procedure, post-fixed in 1% osmate in water and stained with uranyl and lead citrate; 0.1 μm section, d) rat kidney tissue perfused with 0.1 M oxalate *in vitro*, sliced and freeze-dried on a copper grid, e) rabbit spinal cord embedded without staining, 0.5 μm section, f) 0.2 ml of 3 x 10^{-4} M ouabain injected into anterior chamber of rabbit eye; cornea fixed in 1% OsO_4 plus 2% $KSb(OH)_6$ and stained with uranyl and lead acetate; 0.1 μm section. Arrows indicate the areas from which spectra were obtained. Bars indicate 10 μm in panels a, b, d and f, 1 μm in panels c and e.

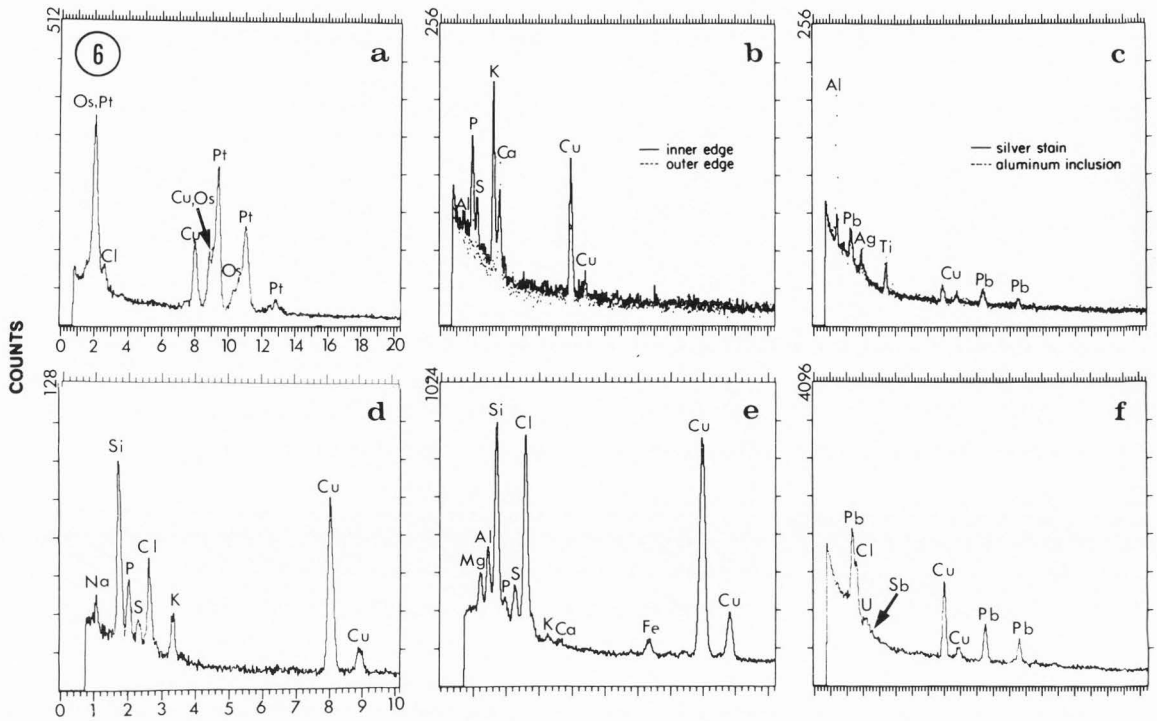
6
a
b
c
d
e
f
COUNTS
Os,Pt
Cl
Cu,Os
Cu
Os
Pt
Pt
Pt
K
P
Ca
S
Al
Cu
Cu
inner edge
outer edge
Al
Pb
Ag
Ti
Cu
Pb
Pb
silver stain
aluminum inclusion
Si
Na
P
Cl
S
K
Cu
Cu
Si
Cl
Al
Mg
P
S
K
Ca
Fe
Cu
Cu
Pb
Cl
U
Sb
Cu
Cu
Pb
Pb

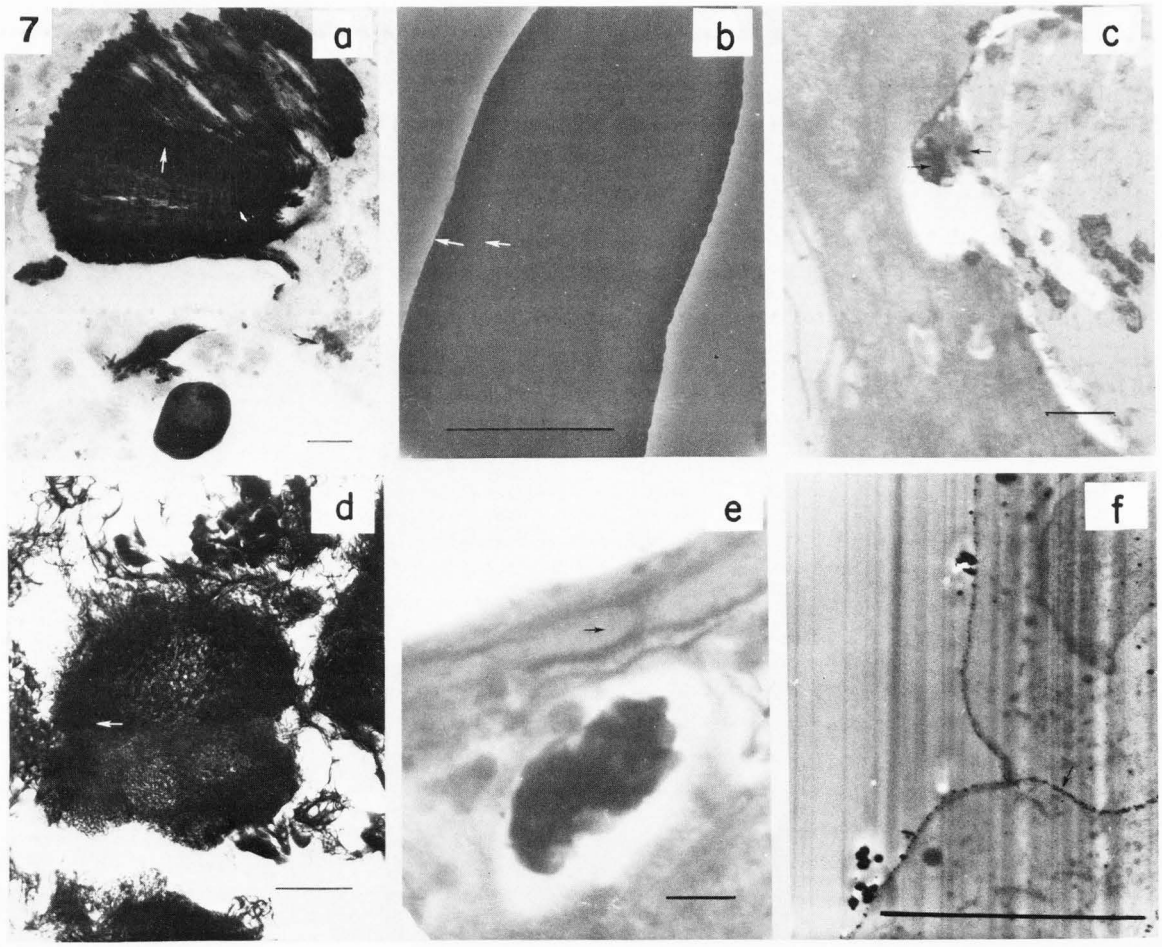
7
a
b
c
d
e
f

monotonically with accelerating voltage. The changes in peak-to-background ratios in Table 3 and in copper-to-aluminum ratios in Table 4 show that although the background increases wih accelerating voltage, the characteristic x-ray production due to multiple scattering decreases with accelerating voltage.

Figures 6 and 7 illustrate the range and utility of XMA on the HVEM. Examination of a large platinum deposit in a thick (1 μm) section and quantitation of the results, currently in progress, will yield evidence of the rates of loss of material from platinum and iridium electrodes (Figs. 6a and 7a). The information sought in this study of the biocompatibility of electrode materials was 1) confirmation that the deposit arose from the electrode, 2) quantitation to determine whether the electrode could be implanted and pulsed with current under the desired operating conditions without losing material at such a rate that either toxic effects or significant changes in effective position would occur over the proposed life of the electrode and, 3) information on the chemical state of material lost from the electrode which might indicate mechanism(s) of loss. This can be obtained by electron diffraction if sufficient order is present or by examination of the ultrastructure for clues.

Differences observed between the inner and outer edges of the skin of an untreated pollen grain more than ten micrometers thick demonstrate the capability to analyse very thick specimens (Figs 6b and 7b). The outer edge shows high calcium and very low potassium, whereas the inner edge shows high potassium and lower calcium. This investigation will examine the effect of ion concentrations on the start of germination. Although the specimen is so thick that no useful electron microscopic image can be obtained, chemical information can distinguish between the skin and the body of the pollen grain.

Spatial resolution is on the order of a fraction of a micrometer as seen by a comparison of the spectra obtained from an aluminum inclusion and a nearby clump of silver stain (Figs. 6c and 7c). A rabbit injected with a slurry of aluminum was used to model dialysis dementia. Information about the movement, accumulation and deposition of the injected particles can be combined with observed central nervous system effects to decide if the model is adequate. Fortuitous propinquity of an aluminum particle to the clump of stain allowed a test of the spatial resolution of the apparatus. Although our probe size is about 0.5 μm and the spectra were obtained 0.25 μm apart, there is partial spatial resolution of the two features.

Thick samples of freeze-dried tissue can be examined readily (Figs. 6d and 7d). This study attempted to determine the initial events leading to the formation of kidney stones. Crystalline features were examined by electron diffraction and XMA to see if they consisted of calcium oxalate and what the hydration state was. This spectrum was obtained from a region in which there was little or no calcium. The silicon peak is an artifact of the preparation method and arises from a glass slide on which the tissue and grid were placed for freeze-drying; the other peaks are as expected for this specimen (the copper comes from the grid).

Embedding unstained tissue need not perturb ion distributions of interest if these ions are not soluble in resin-forming solutions and the preparation necessary for embedding (if any) does not of itself perturb these distributions. Figs. 6e and 7e were obtained from a section of rabbit brainstem and spinal cord which had been embedded without staining. The origin of the silicon peak is unknown, but is probably an artifact. Some of the chlorine undoubtedly comes from the resin, and sodium and potassium have been lost. However, aluminum and iron seem to be well retained, although comparison with a cryo-sectioned, unembedded control is necessary to confirm this. This specimen is part of the same experiment as that in Fig. 6c and was prepared by the same investigator.

The last of this group of specimens is a worst-case tracer analysis (Figs. 6f and 7f). Although the preparation is a thin section, the element of interest occurs in very small particles (compared to our probe size), and there is interference from a nearby peak due to the uranyl stain, the pyroantimonate tracer is detectable. Data from this grid was originally obtained (Kaye et al., 1965) at 10, 20, and 30 keV on a scanning electron microscope equipped with XMA. The smaller probe size allowed better isolation of the feature of interest than we can obtain, and the greater cross-section of x-ray production combined with the much lower brehmsstrahlung background gave a higher signal-to-noise ratio. Nonetheless, the fact that we can (barely) detect the tracer means that experiments using the advantages of both SEM and HVEM may be planned with a reasonable degree of confidence that the information obtained from both instruments can be combined. For example, cutting alternating 25 nm and 1 μm sections, examining the thin sections with SEM and the thick sections with HVEM would allow a small probe to give spatially very accurate chemical information on the thin sections while stereo pairs of the thick sections would allow three-dimensional ultrastructural information to be obtained.

The diameter of our probe, about 0.5 μm, (see Fig. 5), is not especially small since no special modifications have been made to the illumination system of the microscope. However, beam broadening limits the minimum attainable diameter of the analysis volume to approximately 0.1 μm at 1 MV for specimens of several microns thickness (Goldstein et al., 1977). Since the major emphasis in our laboratory is to develop capabilities unique to the HVEM, we will be measuring such thick specimens, thus narrowing the diameter of our probe is of secondary importance.

Future Directions

Although XMA is presently useful on our HVEM, our background is still too high for us to achieve the sensitivity predicted by theory. Theory predicts that the sensitivity of x-ray microprobe analysis will be better at 1000 kV than at 100 kV (Nasir, 1976; Goldstein et al.,

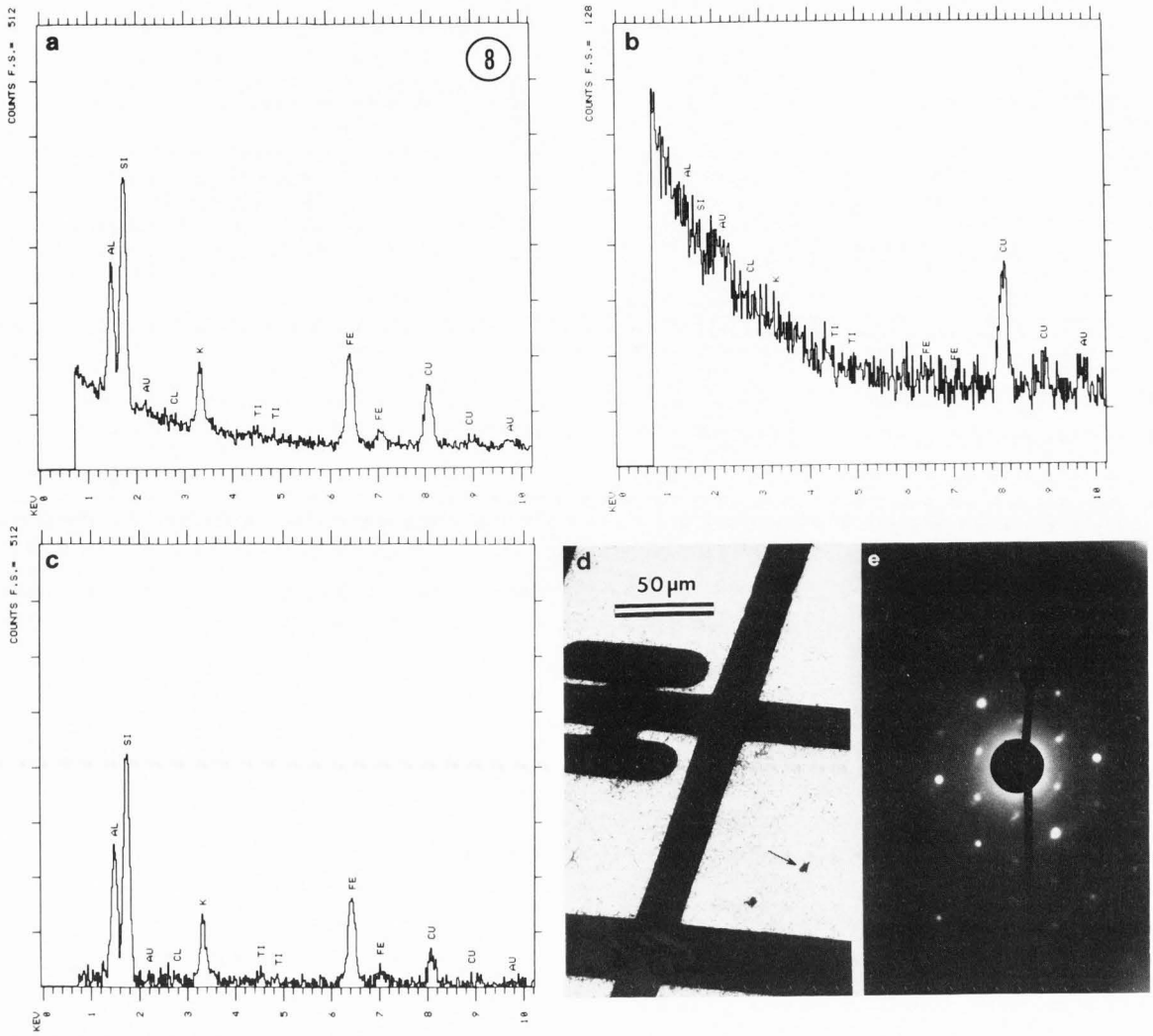

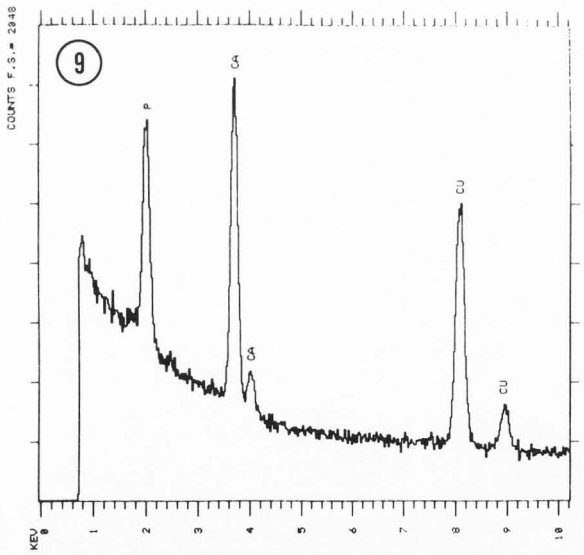

Figure 8. (Above) Air pollution particulate collected on carbon-coated millipore filter, then recoated with carbon, filter dissolved away and carbon sandwich placed on grid. a) Spectrum of particulate, b) spectrum taken about 1 µm from particulate, c) spectrum "b" subtracted from "a", d) low (250x) magnification image of particulate, e) electron diffraction pattern of particulate (camera length is 3.15 m).

Figure 9. (Left) Spectrum of a lithium borate glass standard for potassium and calcium (Fiori and Blackburn, 1982).

1977) due to three effects: 1) the mean square scattering angle for the electron beam is smaller, giving both a smaller effective probe size and a larger electron flux density for a given beam current, 2) the brehmsstrahlung background is more forward peaked, resulting in less overlap with the isotropic characteristic x-ray emission, 3) thicker sections can be analyzed, which means that a given minimum detectable mass corresponds to a lower concentration. We expect work in progress on shielding will allow our experimental

results to reflect this theoretical advantage. Most or all of the stray radiation is produced at the C2 aperture, which defines the beam. A shield has been designed and is being assembled which should absorb this stray radiation more effectively than the present configuration. This shield consists of about 4.5 mm (3/16") of beryllium with a hole of nominal 150 μm diameter atop a lead disk of equal thickness with a hole of nominal 300 μm diameter. This shield will replace the aluminum disk and one or two lead disks presently in use. The beryllium is thick enough to stop electrons whose initial energy is greater than 1.2 MeV giving minimal brehmsstrahlung production (Berger and Seltzer, 1964), and the lead will reduce to 5% or less the intensity of x-rays of energy about 430 keV or less. X-rays of energy less than 300 keV are essentially eliminated by the lead (Forsythe, 1964). Since the intensity of brehmsstrahlung photons of energy E is a constant times (E_o-E) (Compton and Allison, 1935) where E_o is the initial electron energy, there will still be some very high energy photons entering the specimen area. Since it takes 32 mm of lead to reduce the intensity of 1 MeV photons to 5% of the initial intensity (Forsythe, 1964), spatial constraints limit the effectiveness of shielding against such photons. Fortunately, ionization cross-sections for such photons are small, so they will contribute little background to the x-ray spectra.

Replacement of the platinum C2 aperture with a low-Z material is possible, but the intense electron beam imposes constraints on the properties of aperture materials. Beryllium may be suitable since it is an excellent conductor of heat and electricity and has a high melting point. We must, however, be certain that no danger to the personnel or equipment would be posed by using beryllium apertures. The possibility of producing submicron beryllium particles or vacuum evaporating beryllium onto the microscope column would eliminate this material from consideration for use in apertures. Since carbon would likely undergo erosion in the beam (Davy, J, Personal communication) the next low-Z material which might possibly be suitable for apertures is aluminum. Although aluminum has excellent thermal and electrical conductivities also, its melting point is quite low which may be a problem for use as an aperture. We will try aluminum if beryllium would be dangerous.

If after these two improvements there is still too much background, improvements in shielding the specimen area will be tried. Although presently we see little or no background arising from the specimen area, a small source might be revealed when shielding of the upper part of the microscope has eliminated the larger source.

Once we have reduced the background to the point that the theoretical sensitivity has been obtained in practice, we will compile a library of standard spectra. The standards provided by C.E. Fiori (Fiori and Blackburn, 1982) contain most of the elements of interest. Sections of these standards 1 μm thick will be prepared and analysed, and the spectra will be stored. From time to time, standards will be re-analysed and comparisons made between the new and old results to determine any instrumental changes. Those elements not available in lithium borate glass will be dispersed uniformly throughout resin blocks. We have already prepared such blocks for platinum, iridium and mixtures of the two using acetylacetonate complexes obtained from Strem Chemicals, Inc. These complexes are soluble in Epon so the resulting blocks have the required uniform distribution. Comparisons between resin standards and lithium borate glass standards can be used to determine whether matrix corrections are significant.

Other HVEM's on which XMA has been installed have used a geometry where the detector is positioned above the objective lens upper pole piece. This configuration allows the detector to come no closer than 30 mm to the specimen. Our geometry allows a larger signal to be obtained; however, the background is expected to be higher in our geometry.

We have been less successful reducing the background for EELS, and at present no useful results can be obtained. A digital lens current control system is being constructed which will allow the use of P3 to focus the probe on the spectrometer entrance slit. This will demagnify the probe image and improve both the resolution and positional stability. A bending magnet is being designed which will allow the placement of the EELS beam stop at a greater distance from the detector than is now possible. It is expected that these improvements will make EELS useful for our instrument.

Our instrument is also being fitted with a differentially-pumped environmental chamber to allow EELS to be used on hydrated specimens. This will eliminate artifacts produced by standard specimen preparation techniques (Parsons, 1974; Parsons et al., 1974; Morgan, 1979; Panessa-Warren, 1979; King et al., 1980).

Comparisons between our geometry and that used at other HVEM installations and between HVEMs and 100 kV microscopes will be made to determine the types of specimen for which XMA on the HVEM is advantageous and the types for which each of the two geometries offers advantages. To this end, specimens of a few standards have been sent to other HVEMs and to a 100 kV installation.

Acknowledgements

This work is supported by the Department of Health and Human Services under grant number 5 R01 GM28614-03. The New York State high voltage electron microscope facility is supported as a National Biotechnology Resource by the Division of Research Resources, Department of Health and Human Resources, under grant number RR01219.

The authors wish to thank C. Fiori for providing samples of his biological x-ray standards.

References

Bambynek W, Crasemann B, Fink RW, Freund HU, Mark H, Swift CD, Price RE, Rao PV (1972) X-ray fluorescence yields, Auger and Coster-Kronig transition probabilities. Rev. Mod. Phys. 44:716-813.

Barnard D, Ratkowski AJ, Tivol WF (1983) A wire detector for MeV electrons. 7th Int. Conf. HVEM, LBL 16031, Lawrence Berkeley Laboratory, Berkeley, CA, 113-115.

Bentley J, Zaluzec NJ, Kenik EA, Carpenter RW (1979) Optimization of an analytical electron microscope for x-ray microanalysis: Instrumental problems. Scanning Electron Microsc. 1979; II: 581-594.

Berger MJ, Seltzer SM (1964) Studies in Penetration of Charged Particles in Matter. Publication 1133, National Academy of Sciences. National Research Council, Washington, D.C.

Chandler JA (1979) Principles of x-ray microanalysis in biology. Scanning Electron Microsc. 1979; II: 595-606, 618.

Cliff J, Nasir MJ, Lorimer GW, Ridley N (1978) X-ray microanalysis of thin specimens in the transmission electron microscope at voltages up to 1000 kV. 9th Intl. Cong. Elec. Microsc., Toronto, Microscopical Society of Canada, Toronto, Ontario, I:540-541.

Compton AH, Allison SK (1935) X-Rays in Theory and Experiment, 2nd Edition, Chapter II, Section 20. Van Nostrand Co., Inc. Princeton, NJ.

Fiori CE, Blackburn DH (1982) Low-Z glass standards for biological x-ray microanalysis. J. Microsc. 127: 223-226.

Forsythe WE (1964) Smithsonian Physical Tables, 9th revised edition, Table 764 page 693, Smithsonian Institution, Washington, D.C.

Goldstein JI, Costley JC, Lorimer GW, Reed SJB (1977) Quantitative x-ray analysis in the electron microscope. Scanning Electron Microsc. 1977; I: 315-323.

Headley TJ, Hren JJ (1978) Sources of background x-radiation in analytical electron microscopy. 9th Intl. Cong. Elec. Microsc., Toronto Microscopical Society of Canada, Toronto, Ontario I: 504-505.

Jackson JD (1962) Classical Electrodynamics. Chapter 15. Wiley, New York.

Kaye GI, Cole JD, Donn A (1965) Electron microscopy: Sodium localization in normal and ouabain-treated transporting cells. Science 150: 1167-1168.

King MV, Parsons DF, Turner JN, Chang BB, Ratkowski AJ (1980) Progress in applying the high-voltage electron microscope to biomedical research. Cell Biophysics 2: 1-95.

Kobenstuedt H (1967) Simple theory for k-ionization by relativistic electrons. J. Appl. Phys. 38:4785-4787.

Morgan AJ (1979) Non-freezing techniques of preparing biological specimens for electron microprobe x-ray microanalysis. Scanning Electron Microsc. 1979; II: 635-648.

Nasir MJ (1976) X-ray analysis without the need for standards. J. Microsc. 108: 79-87.

Panessa-Warren BJ (1979) Identification and prevention of artifacts in biological x-ray microanalysis. Scanning Electron Microsc. 1979; II: 691-702.

Parsons DF (1974) Structure of wet specimens in electron microscopy. Science 186: 407-414.

Parsons DF, Matricardi VR, Moretz RC, Turner JN (1974) Electron microscopy and diffraction of wet unstained and unfixed biological objects, in: Advances in Biological and Medical Physics, Lawrence JH, Gofman JW and Hayes TL (eds.), Academic Press, NY, 161-270.

Rieder CL, Rupp G, Bowser SS (1984) Electron microscopy of semi-thick sections: advantages for biomedical research. J. Electron Microsc. Techniques, in press.

Zaluzec NJ (1978) Optimizing conditions for x-ray microchemical analysis in analytical electron microscopy. 9th Intl. Cong. Elec. Microsc., Toronto Microscopical Society of Canada, Toronto, Ontario I: 548-549.

Discussion with Reviewers

J.M. Cowley: It is known that hydrated specimens in environmental chambers usually constitute very thick specimens. EELS on the other hand is known to be of value mostly for thin specimens. What is the effective thickness (e.g. equivalent thickness of carbon) for your environmental cell at useful pressures of water vapor and will this thickness limit the effectiveness of the EELS analysis?

Authors: The vapor pressure for 100% humidity at 16°C is 1.8 kPa (J.N. Turner, C.W. See, A.J. Ratkowski, B.B. Chang and D.F. Parsons, Design and operation of a differentially pumped environmental chamber for the HVEM. Ultramicrosc. 6 (1981) 267-280). This gives a mass thickness for water vapor of about 5 $\mu g/cm^2$, which is negligible. The film of water which inevitably covers the specimen is less than 10 nm thick (S. Basu and D.F. Parsons, New wet-replication technique. I. Replication of water droplets. J. Appl. Phys. 47 (1976) 741-751 and S. Basu, G. Hauser and D.F. Parsons, New wet-replication technique. II. Replication of various wet specimens. J. Appl. Phys. 47 (1976) 752-761) giving a mass thickness of less than 1 $\mu g/cm^2$. These thicknesses are small in comparison to both the plasmon mean-free-path (about 20 $\mu g/cm^2$) and the mass-thickness of a wet cell (about 100 $\mu g/cm^2$ for a very thin cell -- about 1 μm thick). The thickness limitation for EELS is, therefore, set by the sample itself rather than the attendant water.

J.M. Cowley: Since water vapor has a low absorption and scattering power for X-rays would it be possible to do useful X-ray EDS analysis of specimens in environmental cells?

Authors: It is certainly possible in principle to obtain useful EDS analyses in an environmental chamber. In practice the design of the chamber must incorporate either a fitting for the detector snout or an additional pair of apertures. In the first case, the environmental chamber is useful only for EDS. Since a reproducibly good seal is impractical, the detector must be left in place and would be damaged during normal EM imaging operation. It was decided not to incorporate a third set of apertures in the environmental chamber presently under construction due to engineering considerations, but possibly a subsequent chamber will incorporate this feature.

J.M. Cowley: The statement in the Discussion section that the diameter of the analysis volume

is on the order of 1 μm for 20 keV electrons and larger for higher energies presumably refers only to very thick specimens. Is it not correct that the diameter of the analysis volume will be much smaller than this for reasonably thin transmission specimens and will decrease for higher energies?
Authors: Yes. A look at the appropriate equation, $b = 625 \frac{Z}{E_o}\left(\frac{\rho}{A}\right)^{\frac{1}{2}} t^{3/2}$ (Text reference Goldstein et al., 1977) yields about 15 nm broadening at 1 MeV for a thickness of 1 μm and 150 nm broadening at 1 MeV for a thickness of 5 μm. Since the primary advantage of element analysis at high voltage is the ability to examine thick specimens, the point that reducing our probe size is of questionable utility is still valid.

G.M. Roomans: Nicholson et al. (J. Microscopy 125, 25-40 (1982)) pointed out the importance of electrons backscattered from below the specimen for the extraneous background. Have the authors considered the relevance of this phenomenon for their system?
Authors: The rather large angle subtended by the bore of the lower objective pole piece, about 0.1 radian, and the forward-peaked distribution of scattered, relativistic electrons result in a condition that the electrons will pass through the bore in the pole piece before back-scattering and hence do not affect our system. However when an objective aperture -- designed to interact with scattered electrons -- is inserted, the dead-time becomes 100% even with the detector retracted. Therefore, when there is anything below the specimen from which electrons can be back-scattered, the background is intense, but when there is not, no background from this phenomenon is observed.

G.M. Roomans: In figure 6f, are the authors certain of the identification of the precipitate as sodium- (rather than calcium-)pyroantimonate, and are they certain that the peak marked Sb is not a convoluted Sb/Ca peak?
Authors: The spectrum shown in figure 6f is from an ouabain-treated preparation; a control preparation -- which should have the same Ca^{++}-distribution -- exhibits considerably reduced precipitate, so at least a great majority of the precipitate must be sodium pyroantimonate. We estimate this to be 90% based on the figures in Kaye et al. (1965). In any case, the point is still valid that the precipitate gives a detectable x-ray signal even though the specimen is ill-suited for the HVEM.

C.E. Fiori: Have the authors attempted to theoretically predict the characteristic to continuum ratios for the various geometrical arrangements in their instrument? If so which cross sections were used and how far off are their measured values from the prediction?
Authors: No, since we are unaware of measurements or calculations of characteristic or continuum cross sections suitable for the experimental conditions on the HVEM. Although only valid for order of magnitude for large angles, Jackson's Classical Electrodynamics equation (15.34) predicts $10^{-2} \ln\left(\frac{885}{E_\gamma(\text{KeV})}\right)$ per 20 eV channel (for electron energy = 1022 keV ($= 2m_e c^2$), $\bar{Z} = 7$, $\theta = 75^o$, collection solid angle of 0.035 sr, 3.35×10^{22} atoms/m^2 (corresponding to a 1 μm thick sample of specific gravity = 1), and 10^{10} electrons/sec incident beam current) or about six counts/channel for a 100 sec. collection time. We actually see about ten times this rate.

Reviewer IV: I believe I am correct in saying that a smaller C2 aperture (say .07 mm) will give a smaller spot on the sample and less current. Was this tried or was it too hard to make the special apertures this size?
Authors: You are correct; a smaller C2 aperture will give a smaller, less intense spot. We do not use special apertures; those which were tested did not prove to reduce the background. Platinum apertures smaller than .25 mm give higher brehmsstrahlung and stray electron background because more of the beam interacts with the aperture material, and they are, therefore, no improvement in our machine. A beryllium-lead shield for the column is being manufactured and some failed attempts to drill a .15 mm hole might be salvaged as small-bore C2 beryllium apertures if possible.